City Research Online

City, University of London Institutional Repository

This is the accepted version of the paper.

This version of the publication may differ from the final published version.

Coupled thermo-mechanical damage modelling for structural steel in fire conditions

Weimiao Lu [1], Cedric D'Mello [2], Ashraf Ayoub [3]

ABSTRACT

This paper aims at developing a coupled thermo-mechanical damage model for structural steel at elevated temperatures. The need for adequate modelling of steel deterioration behaviour remains a challenging task in structural fire engineering because of the complexity inherent in the damage states of steel under combined actions of mechanical and fire loading. A fully three-dimensional damage-coupled constitutive model is developed in this work based on the hypothesis of effective stress space and isotropic damage theory. The new coupling model, adapted from an enhanced Lemaitre's ductile damage equation and taking into account temperature-dependent thermal degradation, is a phenomenological approach where the underlying mechanisms that govern the damage processes have been retained. The proposed damage model comprises a limited number of parameters that could be identified using unloading slopes of stress-strain relationships through tensile coupon tests. The proposed damage model is successfully implemented in the finite element software ABAQUS and validated against a comprehensive range of experimental results. The damage-affected structural response is accurately reproduced under various loading conditions and a wide temperature range, demonstrating that the proposed damage model is a useful tool in giving a realistic representation of steel deterioration behaviour for structural fire engineering applications.

[1] PhD, Department of Civil Engineering, School of Mathematics, Computer Science and Engineering, City, University of London, London, UK, E-mail: Weimiao.Lu.1@city.ac.uk

[2] Professor, Department of Civil Engineering, School of Mathematics, Computer Science and Engineering, City, University of London, London, UK, E-mail: C.A.Dmello-1@city.ac.uk

[3] (Corresponding author) Professor, Department of Civil Engineering, School of Mathematics, Computer Science and Engineering, City, University of London, London, UK, E-mail: Ashraf.Ayoub.1@city.ac.uk

INTRODUCTION

The behaviour of structural steels under high temperatures have been studied by means of high-temperature tensile coupon tests in extensive research works including Skinner (1973), Uddin and Culver (1975), Kirby and Preston (1988), Cooke (1988), Sakumoto (1999), Poh (2001), Outinen and Mäkeläinen (2004), and Chen et al. (2006). A comprehensive review of the high-temperature test data and constitutive models available can be found in Kodur et al. (2010), Luecke et al. (2011) and Kodur and Harmathy (2016). The severe deteriorating effects of high temperatures have also been well recognized by design codes, and the simplified representations of temperature-dependent degradation behaviour of steel provided in ASCE (1992) and EN 1993-1-2 (2005) have been widely adopted for structural fire safety design. However, the behaviour of steel under high temperatures is a complex phenomenon and the deterioration in steel depends not only on elevated temperatures but also on strain levels. It is observed experimentally that the deterioration is more severe at increasing levels of plastic deformation (Pauli et al. 2012). This fact can be attributed to the interactive development of all the processes involved due to simultaneous high temperatures and strains, which leads to the need of sophisticated modelling of steel deterioration behaviour in fire events.

Continuum damage mechanics (CDM) has been commonly used for representing the growth of microdefects and fracture of bonds in steel. An important aspect of continuum damage mechanics is the concept of effective stress which maps stress onto the damaged surface. Kachanov (1958) first came up with a definition of a scalar variable which represents loss of effective resisting area. This has been the starting point for development of damage mechanics models including Lemaitre (1985), Chaboche (1988), Simo and Ju (1987), Chow and Wang (1987), Chandrakanth and Pandey (1993), Bonora (1997), and Bonora et al. (2004). Although CDM has been extensively used in describing the damage mechanisms at ambient temperatures, the development of damage models for steel has not quite been extended to elevated temperatures. Existing work that has dealt with thermo-mechanical damage coupling includes studies on metalworking (Lestriez et al. 2004; Saanouni et al. 2011) and thermal-mechanical fatigue (Velay et al. 2006; Razmi 2012; Egner

2

and Egner 2016). There remains a lack of research which accurately simulates steel deterioration behaviour in fire events by considering the combining effects of mechanical and thermal damage. As a result, research efforts are still required to fill the gap by developing sophisticated models of steel deterioration at high temperatures for applications in structural fire engineering.

Set against this background, this paper focuses on the coupled effects of mechanical and thermal damage on steel deterioration behaviour. The principle features of the framework of CDM that are used to develop the new damage model in this paper are briefly introduced in the next section. In the subsequent sections, a coupled thermo-mechanical damage model is developed based on an enhanced Lemaitre damage model and extended to include temperature dependence, followed by the introduction of the numerical aspects and implementation of the proposed damage model in the FE software ABAQUS/ Explicit. Numerical validations with a comprehensive set of experimental results which verify the predictive capabilities of the proposed damage model and its suitability for use in structural fire engineering simulations are then presented.

PRINCIPLE FEATURES OF CONTINUOUS DAMAGE MECHANICS

In this section, the principle features of the framework of CDM initially proposed by Lemaitre (1985) that are used to build a new damage model in this paper are briefly introduced.

Effective stress concept From a physical point of view, damage is interpreted as a state variable that represents the effects of microvoids on a volume element. Consider a damaged body in a Representative Volume Element (RVE) loaded by a force $\boldsymbol{F}$, let A be the total section area of the RVE defined by its normal $\boldsymbol{n}$ and let A_D be the total area of the microvoids in that section. The isotropic damage variable D can be defined as the effective surface density of microdefects, and the effective stress $\widetilde{\boldsymbol{\sigma}}$ relates to the effective load resisting section area (Kachanov 1958):

$$\widetilde{\boldsymbol{\sigma}} = \frac{\boldsymbol{F}}{A - A_D} = \frac{\boldsymbol{\sigma}}{1 - D} \tag{1}$$

where $\boldsymbol{\sigma} = \boldsymbol{F}/A$.

Any strain constitutive equation may be derived in the same way except that the effective stress replaces the stress in the undamaged material:

$$\epsilon_e = \frac{\widetilde{\sigma}}{E} = \frac{\sigma}{(1-D)E} \tag{2}$$

where ϵ_e is the elastic strain and E is Young's modulus.

Note that taking $\widetilde{E} = (1-D)E$ as the elastic modulus of the damaged material allows one to derive damage variable through $D = 1 - \widetilde{E}/E$.

Coupling between strains and damage In order to derive damage-coupled constitutive equations, the elastic potential Ψ^E is written as quadratic in $\boldsymbol{\varepsilon}^e$ and linear in $(1-D)$ (Lemaitre 1985):

$$\Psi^E(\boldsymbol{\varepsilon}^e, D) = \frac{1}{2}\boldsymbol{\varepsilon}^e : (1-D)\boldsymbol{C} : \boldsymbol{\varepsilon}^e \tag{3}$$

which gives the damaged elasticity law:

$$\boldsymbol{\sigma} = \frac{\partial \Psi^E}{\partial \boldsymbol{\varepsilon}^e} = (1-D)\,\boldsymbol{C} : \boldsymbol{\varepsilon}^e \tag{4}$$

and the damage strain energy release rate:

$$Y = -\frac{\partial \Psi^E}{\partial D} = \frac{1}{2}\boldsymbol{\varepsilon}^e : \boldsymbol{C} : \boldsymbol{\varepsilon}^e = \frac{\sigma_{eq}^{2}R_v}{2E(1-D)^2} \tag{5}$$

where $\boldsymbol{\varepsilon}^e$ is the elastic strain tensor, $\boldsymbol{C}$ is the standard elasticity tensor, σ_{eq} is the von Mises equivalent stress for plasticity, $R_v = 2/3(1+v) + 3(1-2v)(\sigma_H/\sigma_{eq})^2$ is the triaxiality function, σ_H is the hydrostatic stress.

4

Ductile damage evolution The existence of a dissipation potential is assumed as a scalar convex function of state variables Ψ^* $(Y, \dot{p})$, from which damage growth rate $\dot{D}$ is derived (Lemaitre 1985):

$$\dot{D} = -\frac{\partial \Psi^*}{\partial Y} = \begin{cases} 0, & p \leq p_D \\ (\frac{Y}{S})^s \dot{p}, & p > p_D \end{cases} \tag{6}$$

where S is the damage strength, s is the damage exponent, $\dot{p}$ is the equivalent plastic strain rate, p is the equivalent plastic strain measure, p_D is the damage strain threshold.

Enhanced Lemaitre's damage model Bouchard et al. (2011) proposed an enhanced Lemaitre's damage model through modifying the damage potential by adding a term of equivalent plastic strain:

$$\dot{D} = -\frac{\partial \Psi^*}{\partial Y} = \begin{cases} 0, & p \leq p_D \\ (\frac{Y}{S})^s \frac{\dot{p}}{p^r}, & p > p_D \end{cases} \tag{7}$$

Note that when $r = 0$, Eq.7 is identical to Lemaitre's damage model. As $s = 1$ has been suggested by Lemaitre and Chaboche (1994) to give best results when compared to the cavity growth models of McClintock (1968) as well as Rice and Tracey (1969), the enhanced damage model can thus be written as:

$$\dot{D} = -\frac{\partial \Psi^*}{\partial Y} = \begin{cases} 0, & p \leq p_D \\ \frac{\sigma_{eq}{}^2 R_v}{2ES(1-D)^2} \frac{\dot{p}}{p^r}, & p > p_D \end{cases} \tag{8}$$

DEVELOPMENT OF A COUPLED THERMO-MECHANICAL DAMAGE MODEL

This section proposes a new thermo-mechanical scalar damage model based on an enhanced Lemaitre damage model proposed by Bouchard et al. (2011) and extended to take into account high-temperature effects. Two damage component variables d and $h(T)$, associated respectively with mechanical damage and thermal damage processes, are introduced first. The mechanical damage parameter d describes the stiffness degradation caused by the micro-fracturing that develops under

5

mechanical loading, and the thermal damage parameter $h(T)$ accounts for the thermally induced degradation of stiffness. Assuming that the two damage mechanisms act in an interactive way, we define one non-decreasing scalar damage variable D in this paper, which is interpreted as the total density of material defects. In order to describe the interactive development of thermo-mechanical damage, new variables that feature an accelerated damage growth pattern are introduced. Verification of the proposed damage model is then presented which shows that this new damage model is able to reproduce the damage development in steel subjected to a combination of elevated temperatures and mechanical loads.

Mechanical damage component

The damage evolution equation (Eq.8), proposed in the enhanced Lemaitre's damage model (Bouchard et al. 2011), is used to derive mechanical damage component in this paper. The ductile damage is assumed to occur only when the plastic strain threshold is reached and the strain hardening saturates. The von Mises yield criterion in the presence of damage is expressed by means of effective quantities as $\sigma_{eq}/(1-d) - \sigma_s = 0$, where σ_s is saturated yield stress. Thus, with the simplifying assumption that the triaxiality function R_v is constant during the loading process ($R_v = 1$ under uniaxial loading), the mechanical damage component d is integrated as:

$$d = \begin{cases} 0, & p \leq p_D \\ \frac{\sigma_s{}^2}{2ES} R_v (p - p_D)^{1-r}, & p > p_D \end{cases} \tag{9}$$

Thermal damage component

Temperature-dependent elastic modulus reported in tensile coupon tests, which are generally measured at very low strains and defined as the initial slope of the stress-strain curve, are used to determine thermal degradation $h(T)$ in mechanically undamaged steel through relation between reduced elastic modulus $E_0(T)$ and the initial one E_0. Thus, the thermal damage variable $h(T)$ is defined as $h(T) = 1 - E_0(T)/E_0$ and plotted as a function of temperature based on experimentally determined reduction factors (Fig.1). It can be seen from the graph that the thermal damage values derived from different literature sources show some variations but have a common characteristic of

exponential growth. The variations can be attributed to a number of factors such as the differences in steel grades, test regimes and heating methods. Despite these differences, an exponential function of temperature is considered to be capable of capturing the key aspects of thermal damage patterns. Therefore, the thermal damage component developed in this paper is written as an exponential form of the maximum attained temperature governing the thermally activated damage process and the shape of the softening curve:

$$h(T) = ae^{\frac{b}{T+c}} \tag{10}$$

where a, b and c are material constants.

In line with the concept of the irreversibility of damage, the thermal damage growth rate $\dot{h(T)}$ is controlled by the following condition:

$$\dot{h(T)} = 0, \ \ if \ \dot{T} \leq 0; \ \ \dot{h(T)} > 0, \ \ if \ \dot{T} > 0 \tag{11}$$

It should be noted that the new thermal damage model proposed here describes phenomenological thermally-induced degradation in a similar manner to the Arrhenius equation $k = Ae^{-E_a/RT}$ (Arrhenius 1889), in which T is the absolute temperature, A, E_a and R are constants. The Arrhenius equation is an empirical relationship which can be used to model the effect of temperature on vacancy diffusion and many other thermally-induced processes/reactions (Connors 1990). By analogy with the Arrhenius equation one may postulate that the proposed thermal damage model characterizes a similar temperature-driven degradation process governed by the exponential law.

In order to confirm the validity of the proposed model, the new thermal damage model is fitted to experimental data presented in Fig.1. The parameters a, b, and c are determined as best-fit values with the method of least squares and the damage evolution predicted by the proposed thermal damage model is plotted in Fig.2. It can be seen from all five subsets of Fig.2 that the new thermal damage model with best-fit parameters is capable of simulating the damage development which agrees well with experimentally determined steel degradation at various temperature levels. The good correlation confirms that the exponential form of thermal damage description allows an

7

accurate prediction of the degradation in elastic modulus at elevated temperatures with the ease in fitting to the data. The proposed thermal damage formulation by means of an exponential equation is therefore a versatile tool to predict the thermal damage development of steel under fire loading.

Coupling between mechanical and thermal damage

The above has dealt with individual mechanical damage component and thermal damage component, respectively. While mechanical damage is determined by the breaking and re-establishing of atomic bonds (Skrzypek and Ganczarski 2013), thermal degradation can be attributed to decreased bond strength as a result of the nucleus of the iron atoms in steel moving apart at elevated temperatures (Kodur et al. 2010). In both cases, the damage process is the result of several different modes of microstructural kinetics, such as movement of dislocations, diffusion of vacancy, and microcracking propagation. It is generally accepted that atomic bond rupture is a thermally activated process, suggesting that a rise in temperature would provoke an accelerated damage processes (Cottrell 1981). For a given material internal state, it is not known what percentage of damage is caused by mechanical or thermal action and what is their mutual effect. By assuming the distribution of the interatomic bonds, dislocations and vacancies are smeared out and homogenized, a total damage variable can be defined. The overall damage is considered as the reduction of the load-resisting elementary area as the number of bonds decreases, which is interpreted as the total density of material defects. In choosing an appropriate form for representing the damage, the proposed coupling model should be a macroscopically homogeneous, phenomenological damage model which reflects the irreversible changes in the material internal state induced by an external supply of work and heat. The number of parameters necessary to capture the whole behaviour should also be minimized for simplicity while maintaining the accuracy in representing the data. We therefore propose a unified damage function in this paper which meets the requirements and couples both the mechanical and thermal damage processes:

$$D = \frac{\sigma_s{}^2}{2ES}(p - p_D)^{(1-r-T_1^m)}H(p - p_D) + ae^{\frac{b}{T+c}}e^{k(p-p_D)H(p-p_D)} \tag{12}$$

8

where $H(p − p_D)$ is Heaviside function controlling the onset of mechanical damage, whose value is zero for a negative input and one for a positive input. E and σ_s are ambient-temperature initial Young's modulus and saturated yield stress, p is plastic strain, p_D is the damage threshold in strain measure, $T_1 = (T − 20)/(T_{mp} − 20)$, T is the maximum attained temperature, T_{mp} is melt point (normally taken as 1500°C), a, b, c, S and r are material constants, m and k are additional variables introduced to account for thermo-mechanical interaction.

Key factors influencing the initiation of damage process are the temperature T and plastic strain p. At room temperature, the thermal damage term $ae^{b/(T+c)}$ always approaches zero and the proposed damage model is reduced to the special case of mechanical damage only. On the other hand, $H(p − p_D)$ is set to zero when $p \leq p_D$, and the proposed damage model is reduced to thermal damage only. The proposed coupling model can therefore be broken down into the strain and temperature spaces with governing equations defined for each regime as below:

$$
D = \begin{cases}
0 & p \leq p_D, T \leq 20°C \\
\frac{\sigma_s^2}{2ES}(p − p_D)^{(1−r)} & p > p_D, T \leq 20°C \\
ae^{\frac{b}{T+c}} & p \leq p_D, T > 20°C \\
\frac{\sigma_s^2}{2ES}(p − p_D)^{(1−r−T_1^m)} + ae^{\frac{b}{T+c}}e^{k(p−p_D)} & p > p_D, T > 20°C
\end{cases}
\tag{13}
$$

The proposed damage model has the valuable feature of incorporating mutual mechanical and thermal effects by introducing coefficients that account for the accelerated growth of damage. Aspects of thermo-mechanical damage interaction are described by including temperature dependency in the power function of plastic strain which characterizes the influence of temperature on mechanical damage development, and by adding exponential dependency of plastic strain in the thermal degradation term which produces the marked acceleration of thermal damage growth at large plastic strains. The coupling effect remains inactivated until the damage threshold is exceeded in both plastic strain measure and temperature measure. In this way, the interaction between mechanical and thermal damage processes is incorporated into modelling of material deterioration in a smoothed manner without the complexity that normally characterises a micromechanics-based

theory. The evolution of damage is non-decreasing since the reduction of effective resisting area of section will continuously increase until material failure. This gives a realistic description of the material response by limiting the scope of the present study to the heating phase. If not experimentally measured, fracture is generally considered to occur when the accumulated damage variable reaches a value of unity.

Verification of the proposed damage model

The effectiveness of the proposed model is ascertained by describing material degradation behaviour reported in Pauli et al. (2012), in which the elastic slope changes were tracked through loading-unloading cycles at increasing levels of strains and temperatures. The experimental identification procedure is discussed and the damage parameter set for the tested steel is identified.

Pauli et al. (2012) performed tensile coupon tests with loading-unloading cycles at temperatures of 20°C, 400°C, 550°C, and 700°C. The heating rate was $10K/min$ during the first heating stage and then decreased to $2K/min$ until reaching the target temperature. After that, the specimens were loaded in uniaxial tension with a strain rate of $0.1\%/min$ while the temperature was held constant. The initial elastic modulus E_0 was taken as the slope of initial elastic branch at ambient temperature, whereas the temperature-dependent elastic modulus E' was determined at small strains as well as at the reloading branches at engineering strain levels of 2%, 5% and 10% as temperature rises. The changes in measured elastic modulus allow for evaluating the damage evolution which reflects the global deterioration induced by both temperature rise and increasing levels of plastic deformation. The damage variable D at each unloading-reloading cycle is computed as $D = 1 - E'/E_0$.

A summary of the tensile coupon test results and derived damage values is given in Table 1. It is clear that the coupled effects of mechanical damage and thermal damage in test series M7, M8 and M9 are evident. At each temperature level the degradation in elastic modulus becomes more pronounced as the strain increases, which justifies the marked acceleration of damage growth brought about by thermo-mechanical damage interaction as featured in the proposed damage model. Note that there is some deviation in the reduction of elastic modulus observed in test series M7, M8 and M9 within a reasonable margin of error. This may be explained by the slight variations

in material properties of different batches of steel and the inconsistency existing in test conditions and measurements in each test.

The proposed damage model is fitted to the experimentally determined damage values in Table 1, from which the following material constants are deduced:

- the damage threshold strain p_D. Due to the difficulty in determining the starting point at which the mechanical damage is activated, the damage threshold strain usually need to be extrapolated. Here a plastic strain threshold of 0.004 is found to be very close to the elastic limit, indicating that the mechanical damage occurs soon after yielding.
- the exponent $1 - r$ in mechanical damage term is dependent on the type of the nonlinear dependency of the plastic strain observed.
- the damage strength S is determined by plotting the damage D versus the accumulated plastic strain p at room temperature.
- the coefficients of thermal damage term a, b, and c are determined by plotting thermal degradation of Young's modulus versus temperatures at small strains.
- the coupling parameters m and k are calibrated last using the method of least squares, with the intention of matching the overall damage evolution with the experimental dataset.

The best fit of parameters for each test series are listed in Table 2. Due to the scatter of test data, the calibrated damage coefficients show slight differences across three test series. A comparison between the damage model prediction and experimental results is presented in Fig.3. It can be seen from the graph that the damage model closely matches the experimental dataset for all cases. Some deviations from experimental values have been expected considering the simplicity of the model and the limited data points for calibration. The good correlation suggests that it is possible to identify the whole damage parameter set even with limited data available.

Based on the assumption that damage is uniformly distributed in the volume, the proposed damage model (Eq.12) can be generalised to the multiaxial isotropic case, except that here p is the equivalent plastic strain computed from three-dimensional stress-strain fields. It should

be noted that for cases in which material triaxiality differs from that of tensile tests, calibration against experimental data at different levels of triaxiality are generally required. However, there does not exist sufficient data to enable calibration of such triaxiality-dependent models at elevated temperatures. As a result, it is not possible to include the effects of triaxial stress fields on damage growth in the present model with confidence. This simplification can be justified given the fact that severe thermal degradation will be dominant at high temperatures and thus, the effects of triaxiality can be assumed insignificant. Despite this limitation, the use of a coupling model adapted from an enhanced Lemaitre's ductile damage equation and taking into account high-temperature thermal degradation is a phenomenological approach where the underlying mechanisms that govern the damage processes have been retained. Therefore, the proposed damage model is considered to exhibit conservative behaviour outside the range of the data it is based on and is sufficiently accurate for representing the coupled thermo-mechanical damage growth in steel. It should be noted that the damage growth during the cooling phase of fire events is not considered in this study and including this effect is beyond the scope of the present damage model.

To summarize, the coupled thermo-mechanical damage model proposed in this section is able to reproduce the damage behaviour of steel induced by simultaneous mechanical loads and fire exposure. Coupled thermo-mechanical analysis of steel structures can be performed with the proposed damage model incorporated in a FE software using the identified material parameters as the basic data.

INTEGRATION SCHEMES

This section introduces the numerical aspects and the implementation of the proposed damage model in the FE software ABAQUS. To enable simulation of successive failures of elements and the subsequent redistribution of loads, the proposed damage model is incorporated into user subroutine VUMAT of ABAQUS/Explicit. Components of the damage-coupled governing constitutive equations and the discretization procedure of the computational model are presented in this section.

12

Constitutive equations

To derive the governing equations of coupled thermo-elasticity and thermo-plasticity in the presence of damage, the expression for the thermo-elastic free energy density Ψ^E proposed by Stabler and Baker (2000) for high temperature increments is used here:

$$\Psi^E(\boldsymbol{\varepsilon^e}, D, T) = \frac{1}{2}\boldsymbol{\varepsilon^e} : (1-D)\boldsymbol{C} : \boldsymbol{\varepsilon^e} - (T-T_0)\boldsymbol{\beta} : \boldsymbol{\varepsilon^e} + c_v[T - T_0 - Tln(\frac{T}{T_0})] \qquad (14)$$

which gives the constitutive stress-strain equation:

$$\boldsymbol{\sigma} = \frac{\partial \Psi^E}{\partial \boldsymbol{\varepsilon^e}} = (1-D)\,\boldsymbol{C} : \boldsymbol{\varepsilon^e} - (T-T_0)\boldsymbol{\beta} \qquad (15)$$

where $\boldsymbol{\sigma}$ is the stress tensor, $\boldsymbol{C}$ is the elastic modulus tensor, $\boldsymbol{\varepsilon^e}$ is the elastic strain tensor, T_0 is the initial temperature, T is a measure of temperature, $\boldsymbol{\beta}$ is the thermo-elastic coupling tensor that represents stress induced by thermal expansion, and c_v is the specific heat.

The yield criterion is formulated in the effective stress space and given as a function of the stress, damage and temperature:

$$f^p(\boldsymbol{\sigma}, R, D, T) = \frac{\sigma_{eq}}{1-D} - \sigma_y(R, T) = 0 \qquad (16)$$

where $\sigma_y(R, T)$ defines the yield surface evolution under thermal and mechanical loading.

The reduction of effective yield strength given in EN 1993-1-2 (2005) has been generally accepted as a fairly good representation of the contraction of yield surface with increasing temperature. However, it is important to note that if the temperature-dependent effective yield strength (EN 1993-1-2 2005) is taken as $\sigma_y(R, T)$ here in the fictitious undamaged configuration, the yield surface inevitably undergoes a further isotropic contraction induced by elevated temperature owing to the fact that the total damage variable D has already taken into account the effects of thermal degradation. Undoubtedly this will lead to an erroneous and over-conservative prediction. Therefore, a modified yield surface is adjusted by precluding the effects of thermal degradation $h(T)$

13

brought about by the total damage D while keeping the reduction factors of yield strength $k_{y,T}$ as specified in EN 1993-1-2 (2005):

$$\sigma_y(R, T) = \frac{\sigma_y(R)}{1 - h(T)} k_{y,T} \tag{17}$$

where $\sigma_y(R)$ is the yield stress at ambient temperature.

The modified yield surface is proposed based on the concept of generalized effective space plasticity and isotropic damage theory, taking into account the effect of high temperature on the mechanical behaviour. By relating different governing parameters to the yield strengths under thermal and mechanical loading, the obtained yield condition hence reflects a combination of the evolution of thermal softening and mechanical degradation and can be used in any temperature and stress states. It also encompasses the capability to yield back the same prescriptive strength reduction as specified in EN 1993-1-2 (2005) in the situation where mechanical damage is not present. The characterization of plastic response is thus formulated by extrapolating the yield surface in three-dimensional principle stress space, with the effects of damage reflected in the accompanying degradation in stiffness and yield strength.

Integration algorithm

The constitutive equations are discretized within the framework of FE method based on the numerical approach presented by Benallal et al. (1988) and de Souza Neto et al. (2011), with the superscripts i and $i + 1$ referring to the beginning and the end of the current increment, respectively. A stable radial return mapping algorithm is used for the integration of damage evolution equation coupled with isotropic hardening plasticity model. The calculations of the stresses and strains are first performed by an elastic predictor assuming the first increment to be purely elastic:

$$\boldsymbol{\sigma_{tr}}^{(i+1)} = \boldsymbol{\sigma}^{(i)} + \lambda(1 - D^{(i)}) trace\,(\Delta\boldsymbol{\varepsilon})\,\boldsymbol{I} + 2G(1 - D^{(i)})\Delta\boldsymbol{\varepsilon_{el}} \tag{18}$$

where $\boldsymbol{\sigma_{tr}}^{(i+1)}$ is the trial stress tensor at the end of the increment, $\boldsymbol{\sigma}^{(i)}$ is the stress tensor at the beginning of the increment, $\Delta\boldsymbol{\varepsilon_{el}}$ is the elastic strain increment, $\Delta\boldsymbol{\varepsilon_{el}} = \Delta\boldsymbol{\varepsilon} - \Delta\boldsymbol{\varepsilon_T}$, $\Delta\boldsymbol{\varepsilon_T}$ is the

14

thermal strain, $trace\,(\Delta\varepsilon)$ is the volume strain increment, I is the identity matrix, λ and G are the Lames constants, and $D^{(i)}$ is the damage variable at the beginning of the increment.

Then the yield function is evaluated:

$$f^p(\sigma, R, D, T) = \frac{q_{tr}^{(i+1)}}{1 - D^{(i)}} - \sigma_y(R^{(i)}, T^{(i)}) \leq 0 \tag{19}$$

where $q_{tr}^{(i+1)}$ is the Von Mises equivalent stress in the elastic trial state, $R^{(i)}$ is the scalar isotropic hardening variable at the beginning of the increment, $T^{(i)}$ is the maximum attained temperature passed into VUMAT at the beginning of the increment and kept constant during the current increment.

If the elastic predictor satisfies the yield criterion, the new stress is set equal to the trial stress. Otherwise, the material point goes beyond the yield surface and the plastic correction is required in which the stress state is returned to the yield surface along the direction of plastic flow:

$$\sigma^{(i+1)} = \sigma_{tr}^{(i+1)} - 2G(1 - D^{(i)})\Delta\epsilon_p \tag{20}$$

where $\Delta\epsilon_p$ is the plastic strain increment which is governed by the plastic flow rule $\Delta\epsilon_p = \Delta\gamma N^{(i+1)}$.

The plastic multiplier $\Delta\gamma$ is obtained by ensuring that the yield condition must be satisfied at the end of the increment:

$$\Delta\gamma = \frac{(1 - D^{(i)})\widetilde{q}_{tr}^{(i+1)} - q^{(i+1)}}{3G} \tag{21}$$

where $\widetilde{q}_{tr}^{(i+1)}$ is the effective elastic predictor, $q^{(i+1)}$ is the von Mises equivalent stress.

The normal vector to the yield surface $N^{(i+1)}$ is given by:

$$N^{(i+1)} = \frac{3}{2}\frac{s^{(i+1)}}{(1 - D^{(i)})q^{(i+1)}} \tag{22}$$

where $s^{(i+1)}$ is the deviatoric stress.

15

The updated damage variable can now be written as:

$$D^{(i+1)} = \frac{\sigma_s{}^2}{2ES}(p^{(i+1)} - p_D)^{(1-r-T_1^m)}H(p^{(i+1)} - p_D) + ae^{\frac{b}{T^{(i)}+c}}e^{k(p^{(i+1)}-p_D)H(p^{(i+1)}-p_D)} \qquad (23)$$

where $p^{(i+1)}$ is the equivalent plastic strain at the end of the increment.

When the damage indicator $D^{(i+1)}$ reaches the critical value D_{cr} (D_{cr} is usually taken as 1 if not experimentally measured), the material point is deleted from the analysis model by setting the stress components to zero for the rest of the analysis.

To summarize, a damage-plasticity model in terms of effective stresses coupled with isotropic damage is implemented in user subroutine VUMAT of ABAQUS /Explicit. It should be noted that the numerical integration algorithm is applicable for solid elements in 3D principal stress space and can easily be extended to 1D beam element and 2D plane stress shell element. Numerical analyses are performed with ABAQUS/Explicit in the next section in order to further verify the predictive capabilities of the proposed damage model and its suitability for use in structural fire engineering simulations.

NUMERICAL VALIDATIONS

This section presents numerical validation studies of the proposed damage model against a comprehensive set of experimental work in which different levels of loads and temperatures are considered.

Steel beam fire test

A simply supported steel I-beam is first studied and compared with the experimental results by Dharma and Tan (2007). Specimen S3-1 was tested at room temperature and specimens S3-2 and S3-3 were heated to 415°C and 615°C at a heating rate of 7°C/min, respectively. The FE model is created in ABAQUS using shell elements S4R, with six elements across the flange width and six elements through the depth of the web based on mesh sensitivity study.

Due to the fact that the tensile coupon tests in Dharma and Tan (2007) did not provide sufficient data for calibrating damage model parameters, the damage parameter sets employed in Table 2 are

16

used as initial estimate in damage-coupled numerical analysis. Simulations performed with the three damage parameter sets show that the load versus displacement curves generated by the parameter set M7 and M8 give poor predictions, whereas M9 parameter set gives excellent experimental fit. It can be seen from Fig.4 that the failure mode and buckling shape are well captured by the numerical analysis with M9 damage parameter set, which matches the ones observed in Dharma and Tan (2007) well. Using the same damage parameter input, the damage model prediction and EC3 model prediction for each loading case in terms of load versus displacement data are presented in Fig.5 along with the test results. Note that the damage propagation behaviour is not included in the EC3 model and the softening in this case is due to geometric nonlinearity.

As can be seen from the load-deflection curves, the damage model predictions and experimental data agree quite well in all cases. The stiffness, strength and deterioration in the overall beam behaviour is well reproduced, which confirms the effect of damage imposed on the behaviour of the steel beam. In particular, the softening branch is simulated with remarkable accuracy, which validates the choice of damage model parameters used in the analysis as these are the governing factors which control the shape of the load-deflection curve in the post-peak softening branch. The evolving damage accounts for the progressive degradation after the damage threshold is exceeded or the removal of elements once the critical damage value is reached at integration points. This is not the case for the EC3 model, which explains the fact that EC3 model predictions overestimate the capacity of the steel I-beams considerably. The curves generated by the two different approaches follow the same path until they reach the critical point of fracture initiation. The curves then start to diverge as the damage variable introduced governs the damage evolution and progressively reduces the Young's modulus and yield strength of material. These results also validate the ability of the damage model to predict the load-carrying capacity before ultimate failure occurs.

Note that there is some discrepancy in the yield strength and hardening branch of specimen S3-2 between the numerical predictions and the experimental data. This is probably due to the difference between the material properties in experiments and FE models and the use of idealised restraints in simulations. Nevertheless, the maximum load is well predicted by the proposed damage model

17

for specimen S3-2. Overall, the results have successfully captured the main trends exhibited in the experimental data and are sufficiently accurate for the current computational exercise. It can be concluded that the calibration of the damage model is successful and the coupled effect of damage and plasticity on the predicted behaviour is evident. The predictions match experimental results fairly well in all cases, indicating the adequacy of the damage model in describing phenomena in both low range and high range of temperatures.

Steel beam-to-column connection fire test

The capability of the damage model approach in simulating damage development, material degradation and subsequent element deletion is also validated through comparison with experimental study of steel flush end-plate beam-to-column connection by Leston-Jones et al. (1997). The test program consisted of: One specimen loaded at room temperature until failure and five others tested in fire at heating rate of $10°$C/min under load level of $5kN \cdot m$, $10kN \cdot m$, $15kN \cdot m$, $20kN \cdot m$ and $25kN \cdot m$, respectively.

The FE model is constructed with three-dimensional solid elements C3D8R. A mesh sensitivity study shows that the appropriate global mesh size for structural components is $10mm$ to $20mm$, while the mesh of the region near the face of the beam-column connection is further refined with a minimum of three layers of elements specified through the plate thickness. The modelling details of connection components are shown in Fig.6, in which a number of contact pairs are specified using ABAQUS surface to surface contact option. "Hard" contact is assumed for the normal behaviour and a friction coefficient of 0.1 is specified for tangential behaviour in contact property definition. The initial gap between the bolt shank and bolt hole is set at 0.1 mm.

The initial estimate for the damage model parameters is identical to that employed in the previous case study (dataset M9 in Table 2). The damage model prediction is consistent with the experimental observations, in which damage is concentrated in the compression web and tension flange of the column. The damage distribution contour and the failure mode of the connection are shown in Fig.7. The similarities between numerical and experimental failure modes confirm that the proposed modelling approach is able to identify the zone of damage propagation.

18

Fig.8 shows a comparison of the connection responses between numerical cases and test results. The predictions of the proposed damage model provide closer fit to experimental results compared to the EC3 model predictions for all cases, particularly in terms of moment capacity at room temperature and failure temperature under fire loading. For the first fire test (moment level of $5kN \cdot m$), both numerical approaches overpredict the temperature corresponding to plastification of the elements within the connection. This may be explained by the fact that the furnace heating might not be as uniform as in numerical simulations. In Fig.8 (b)-(f), the initial stiffness predicted by the damage model is slightly higher than the EC3 model prediction because there is no mechanical damage at this stage and the stiffness is only controlled by $E_0(T)/E_0$. This observation suggests that the EC3 model gives a slightly more significant reduction in Young's modulus than the thermal damage model alone in this case. However, the stiffness and moment capacity of the connection in the damage model prediction are reduced considerably when the coupled thermo-mechanical damage comes into effect at increasing temperatures and extensive plastification. The pattern of structural response at moment level of $10kN \cdot m$ and $15kN \cdot m$ is similar to that observed in the first fire test. On the other hand, the coupled effects of mechanical damage and thermal damage are particularly evident in the case of moment level $20kN \cdot m$ and $25kN \cdot m$. These two cases with high load ratios provide insight closely related to the degradation of connection capacity. Results indicate that the damage model prediction has a nearly perfect fit for the plateau in the connection response upon rapid increase in rotation, whereas the failure of the connection occurs at a significantly higher temperature in EC3 model prediction for moment level of $20kN \cdot m$ and $25kN \cdot m$.

Overall, the proposed damage model manages to predict the failure temperatures within a 5% error margin for almost all loading cases except BFEP10. It is important to note that by making further adjustments in the magnitudes of the damage model parameters, results of some loading cases might be improved at the cost of numerical accuracy in other loading cases. Therefore, judging from the overall performance of the damage model, the employed damage parameters succeed in adequately describing experimental phenomena. To summarize, the proposed damage

19

model has a significant contribution in estimating structural behaviour at high load levels during fire events and it should be incorporated into numerical simulations even for low levels of loading.

Steel tubular truss fire test

In addition to establishing the effectiveness of the damage model approach in modelling connection assembly, the validation attempt also includes study on steel tubular trusses. Liu et al. (2010) conducted fire tests on steel tubular trusses which consisted of two vertical chords, two horizontal braces and two diagonal braces (Fig.9). Two different levels of axial loads were considered, being $400kN$ for specimen SP1 and $600kN$ for specimen SP2.

The FE simulations are carried out in ABAQUS using beam element B21. The temperature histories of truss members are assumed to follow those described in Liu et al. (2010), in which the maximum temperature in the heated members climbs from 20°C to over 800°C in less than 15 minutes. The heating rates employed in this fire test are much faster than the experimental studies discussed earlier. As faster heating rates have considerable impact on the material microstructure (Bednarek and Kamocka 2006), the previously calibrated damage model parameters in Table 2 cannot be used to reproduce the degradation behaviour observed in this study. Due to the lack of coupon data for this particular heating rate, calibration is re-conducted to find the most appropriate damage model parameters through a trial and error procedure. An array of values are initially proposed for the parameters across the possible solution range in the identification process. The optimum solution is obtained through updating the magnitude of each parameter in turn while other parameters are kept fixed in a series of simulations. Using this procedure, parameters a, b and c are first calibrated to match the displacement behaviour at low range of temperatures. Parameters S and r are adjusted to give a better prediction of mechanical damage growth, with the plastic strain threshold p_D determined as the initiation point of mechanical damage. After this, the coefficients m and k which account for the coupled effects of thermo-mechanical damage growth are manipulated to obtain the desirable accelerated damage rates. It is important to note that the rapid loss of load carrying capacity can be premature or delayed by choosing different combinations of these model parameters. This process continues until convergence to the optimal solution has been obtained

after approximately 240 iterations. Results show that the calibrated damage model is able to match the experimental temperature-displacement behaviour fairly well and the failure predictions are within 5% of the experimental results for both specimen SP1 and specimen SP2. The adjusted values for the damage model parameters used for this heating rate are provided in Table 3.

Fig.10 (a) shows that the damage model prediction and EC3 model prediction look very similar for specimen SP1. The failure temperature predicted by both numerical approaches is 645°C, which is slightly lower than 678°C reported in the test. The discrepancies observed may be attributed to possible experimental errors and simplified modelling approximations. The inclusion of a damage model does not exhibit a major impact in this case, suggesting that the structural response of specimen SP1 is mainly governed by the material temperature-dependency and to a lesser extent the contribution of mechanical damage component. The damage propagation resulting from the coupled thermo-mechanical damage development is in relatively small scale compared to the size of the specimen SP1.

Due to a higher level of applied load, the damage growth and therefore the deterioration in load-carrying capacity of specimen SP2 is more pronounced. As a result, the difference between the damage model prediction and EC3 model prediction is more distinguishable in specimen SP2 than in specimen SP1, as shown in Fig.10 (b). The proposed damage model provides an excellent prediction of failure temperature that is identical to the test finding and the predicted displacement matches the test results closely up to the failure temperature. On the other hand, the EC3 model overestimates the failure temperature of the steel truss considerably. This again shows that the coupled effects of mechanical damage and thermal damage are more evident under high load levels.

Discussion

Thus far, the performance of the proposed damage model is illustrated using several benchmark problems under various states of loading and temperatures. Computational results obtained with the proposed damage model correlate well with experimental results, demonstrating the consistent and accurate predictive capabilities of the proposed damage model. Compared to conventional numerical models, the calibrated damage model manages to reproduce the load-displacement

21

behaviour, ultimate failure temperature and failure initiation locations with improved accuracy. It can be concluded that the proposed damage model makes a significant contribution in estimating structural behaviour at high load levels and it should be incorporated into numerical simulations even for low levels of loading. It is observed that the procedure adopted allows for adequate derivation of damage model parameters despite the lack of coupon test data. The calibrated data sets are in a consistent format and depend considerably on the heating rate range. This makes it reasonable to categorize the calibrated damage parameters based on the heating rate (Table 4), which permits applying the proposed damage model to different types of structural fire engineering problems.

One of the advantages with the proposed damage model is that it is fully three-dimensional. Applications of the proposed damage model with a flexible choice of elements, including solid elements, shell elements and beam elements, have been presented in this section. It is observed that the damage model's capability to describe stiffness degradation and capacity deterioration is not affected by the choice of elements, so long as mesh sizes are deemed appropriate according to the mesh sensitivity study. It should be pointed out that the capability of the proposed damage model in terms of practical usefulness and numerical robustness has great potential for future work. For instance, practical applications based on solid elements normally include modelling of beam-to-column connections. On the other hand, shell elements are superior in simulating buckling behaviour and beam elements are commonly used in the analysis of complex structures which might encompass numerous elements.

CONCLUDING REMARKS

This paper presents a new coupled thermo-mechanical damage model that fills the gap in the modelling of steel deterioration for applications in structural fire engineering. Based on the effective stress concept and isotropic damage theory, the proposed damage model is developed in a macroscopically homogeneous, phenomenological form that features mutual strain and temperature effects on damage development. Only a few parameters are used, which makes it easy to use in structural applications. Calibrated damage model parameters are recommended for use in

structural fire engineering simulations based on heating rate ranges. The numerical aspects and the implementation scheme of the proposed damage model are derived based on an elastic predictor and a radial return mapping algorithm. On successful implementation of the user defined damage-coupled material law in ABAQUS, the capability and applicability of the proposed damage model is verified with a comprehensive set of experimental results.

To conclude, the proposed damage model has been developed, calibrated and validated, which successfully fulfils the purpose of this paper. The validity of the proposed model is limited by the hypothesis of multiaxial isotropic damage and multiaxial isotropic plasticity which is representative of structural steels. It should also be mentioned that experimental data on steel deterioration at elevated temperatures are currently insufficient to support the inclusion of the effects of triaxiality, and the current damage model does not further trace the material response after fire enters into its cooling phase. Notwithstanding these limitations, this paper provides a framework for incorporating coupled thermo-mechanical damage modelling of structural steels in FE analysis with currently available tensile coupon data. Numerical validations conducted in this paper serve to illustrate that the proposed damage model provides an important advancement toward giving a realistic representation of steel deterioration behaviour under combined actions of fire and mechanical loads. Such a model with carefully calibrated parameters could thus be employed with confidence in a wide range of structural fire engineering applications. Furthermore, it is recommended that more experimental studies be conducted which will benefit the data collection work for calibrating damage model parameters.

REFERENCES

Arrhenius, S. (1889). "Über die dissociationswärme und den einfluss der temperatur auf den dissociationsgrad der elektrolyte." *Zeitschrift für physikalische Chemie*, 4(1), 96–116.

ASCE (1992). *Structural fire protection*. ASCE Manuals and Reports on Engineering, No. 78, American Society of Civil Engineers.

Bednarek, Z. and Kamocka, R. (2006). "The heating rate impact on parameters characteristic of

steel behaviour under fire conditions." *Journal of Civil Engineering and Management*, 12(4), 269–275.

Benallal, A., Billardon, R., and Doghri, I. (1988). "An integration algorithm and the corresponding consistent tangent operator for fully coupled elastoplastic and damage equations." *International Journal for Numerical Methods in Biomedical Engineering*, 4(6), 731–740.

Bonora, N. (1997). "A nonlinear CDM model for ductile failure." *Engineering fracture mechanics*, 58(1-2), 11–28.

Bonora, N., Gentile, D., and Pirondi, A. (2004). "Identification of the parameters of a non-linear continuum damage mechanics model for ductile failure in metals." *The Journal of Strain Analysis for Engineering Design*, 39(6), 639–651.

Bouchard, P.-O., Bourgeon, L., Fayolle, S., and Mocellin, K. (2011). "An enhanced Lemaitre model formulation for materials processing damage computation." *International Journal of Material Forming*, 4(3), 299–315.

Chaboche, J.-L. (1988). "Continuum damage mechanics: Part II Damage growth, crack initiation, and crack growth." *Journal of applied mechanics*, 55(1), 65–72.

Chandrakanth, S. and Pandey, P. (1993). "A new ductile damage evolution model." *International Journal of Fracture*, 60(4), R73–R76.

Chen, J., Young, B., and Uy, B. (2006). "Behavior of high strength structural steel at elevated temperatures." *Journal of structural engineering*, 132(12), 1948–1954.

Chow, C. and Wang, J. (1987). "An anisotropic theory of continuum damage mechanics for ductile fracture." *Engineering Fracture Mechanics*, 27(5), 547–558.

Connors, K. A. (1990). *Chemical kinetics: the study of reaction rates in solution*. John Wiley & Sons.

Cooke, G. M. (1988). "An introduction to the mechanical properties of structural steel at elevated temperatures." *Fire safety journal*, 13(1), 45–54.

Cottrell, A. H. (1981). *The mechanical properties of matter*. Krieger Publishing.

de Souza Neto, E. A., Peric, D., and Owen, D. R. (2011). *Computational methods for plasticity:*

theory and applications. John Wiley & Sons.

Dharma, R. B. and Tan, K.-H. (2007). "Rotational capacity of steel I-beams under fire conditions Part I: Experimental study." *Engineering structures*, 29(9), 2391–2402.

Egner, W. and Egner, H. (2016). "Thermo-mechanical coupling in constitutive modeling of dissipative materials." *International Journal of Solids and Structures*, 91, 78–88.

EN 1993-1-2 (2005). *Eurocode 3: Design of Steel Structures, Part 1-2: General Rules – Structural Fire Design*. European Committee for Standardization, Brussels, Belgium.

Kachanov, L. (1958). "On rupture time under condition of creep." *Izvestia Akademi Nauk USSR, Otd. Techn. Nauk, Moskwa*, 8, 26–31.

Kirby, B. and Preston, R. (1988). "High temperature properties of hot-rolled, structural steels for use in fire engineering design studies." *Fire safety journal*, 13(1), 27–37.

Kodur, V., Dwaikat, M., and Fike, R. (2010). "High-temperature properties of steel for fire resistance modeling of structures." *Journal of Materials in Civil Engineering*, 22(5), 423–434.

Kodur, V. and Harmathy, T. (2016). "Properties of building materials." *SFPE handbook of fire protection engineering*, Springer, 277–324.

Lemaitre, J. (1985). "A continuous damage mechanics model for ductile fracture." *Journal of Engineering Materials and Technology*, 107(1), 83–89.

Lemaitre, J. and Chaboche, J.-L. (1994). *Mechanics of solid materials*. Cambridge university press.

Leston-Jones, L., Burgess, I., Lennon, T., and Plank, R. (1997). "Elevated-temperature moment-rotation tests on steelwork connections." *Proceedings of the Institution of Civil Engineers-Structures and Buildings*, 122(4), 410–419.

Lestriez, P., Saanouni, K., Mariage, J.-F., and Cherouat, A. (2004). "Numerical prediction of ductile damage in metal forming processes including thermal effects." *International Journal of Damage Mechanics*, 13(1), 59–80.

Liu, M., Zhao, J., and Jin, M. (2010). "An experimental study of the mechanical behavior of steel planar tubular trusses in a fire." *Journal of Constructional Steel Research*, 66(4), 504–511.

Luecke, W. E., Banovic, S. W., and McColskey, J. D. (2011). "High-temperature tensile constitutive

data and models for structural steels in fire." *Report No. 1714*, NIST.

McClintock, F. A. (1968). "A criterion for ductile fracture by the growth of holes." *ASME Journal of Applied Mechanics*, 35(2), 363–371.

Outinen, J. and Mäkeläinen, P. (2004). "Mechanical properties of structural steel at elevated temperatures and after cooling down." *Fire and materials*, 28(2-4), 237–251.

Pauli, J., Somaini, D., Knobloch, M., and Fontana, M. (2012). "Experiments on steel columns under fire conditions." *Report No. 340*, Institute of Structural Engineering (IBK), ETH Zürich, Switzerland.

Poh, K. (2001). "Stress-strain-temperature relationship for structural steel." *Journal of Materials in Civil Engineering*, 13(5), 371–379.

Razmi, J. (2012). "Thermo-mechanical fatigue of steel piles in integral abutment bridges." Ph.D. thesis, University of Maryland, College Park.

Rice, J. and Tracey, D. M. (1969). "On the ductile enlargement of voids in triaxial stress fields." *Journal of the Mechanics and Physics of Solids*, 17(3), 201–217.

Saanouni, K., Lestriez, P., and Labergère, C. (2011). "2D adaptive FE simulations in finite thermo-elasto-viscoplasticity with ductile damage: application to orthogonal metal cutting by chip formation and breaking." *International Journal of Damage Mechanics*, 20(1), 23–61.

Sakumoto, Y. (1999). "Research on new fire-protection materials and fire-safe design." *Journal of Structural Engineering*, 125(12), 1415–1422.

Simo, J. and Ju, J. (1987). "Stress and strain based continuum damage models, parts I and II." *International Journal of Solids and Structures*, 23(7), 841–869.

Skinner, D. (1973). "Steel properties for prediction of structural performance during fires." *Fourth Australasian conference on the mechanics of structures and materials: Proceedings*, 269–276.

Skrzypek, J. J. and Ganczarski, A. (2013). *Modeling of material damage and failure of structures: theory and applications*. Springer Science & Business Media.

Stabler, J. and Baker, G. (2000). "Fractional step methods for thermo-mechanical damage analyses at transient elevated temperatures." *International Journal for Numerical Methods in Engineering*,

607   48(5), 761–785.

608 Uddin, T. and Culver, C. G. (1975). "Effects of elevated temperature on structural members."

609   *Journal of the Structural Division*, 101(7), 1531–1549.

610 Velay, V., Bernhart, G., and Penazzi, L. (2006). "Cyclic behavior modeling of a tempered martensitic

611   hot work tool steel." *International Journal of Plasticity*, 22(3), 459–496.

List of Tables

TABLE 1. Temperature-dependent elastic modulus and damage values determined from tensile coupon test conducted by Pauli et al. (2012)

Test series	Coupon	Temperature(°C)	True strain	$E_0(N/mm^2)$	$E'(N/mm^2)$	Damage
	M7-T02	20	0.000	1.88E+11	1.88E+11	0.000
	M7-T02	20	0.009	1.88E+11	1.66E+11	0.117
	M7-T02	20	0.021	1.88E+11	1.51E+11	0.197
	M7-T02	20	0.041	1.88E+11	1.36E+11	0.277
	M7-T07	400	0.000	2.18E+11	1.77E+11	0.188
	M7-T07	400	0.009	2.18E+11	1.75E+11	0.197
	M7-T07	400	0.021	2.18E+11	1.62E+11	0.257
M7	M7-T07	400	0.041	2.18E+11	1.47E+11	0.326
	M7-T11	550	0.009	2.17E+11	1.23E+11	0.433
	M7-T11	550	0.021	2.17E+11	1.12E+11	0.484
	M7-T11	550	0.041	2.17E+11	1.00E+11	0.539
	M7-T05	700	0.009	2.24E+11	5.87E+10	0.738
	M7-T05	700	0.021	2.24E+11	6.09E+10	0.728
	M7-T05	700	0.041	2.24E+11	5.13E+10	0.771
	M8-T02	20	0.000	2.11E+11	2.11E+11	0.000
	M8-T02	20	0.009	2.11E+11	1.74E+11	0.175
	M8-T02	20	0.021	2.11E+11	1.59E+11	0.246
	M8-T02	20	0.041	2.11E+11	1.42E+11	0.327
	M8-T05	400	0.009	2.06E+11	1.68E+11	0.184
	M8-T05	400	0.021	2.06E+11	1.56E+11	0.243
M8	M8-T05	400	0.041	2.06E+11	1.41E+11	0.316
	M8-T10	550	0.009	2.11E+11	1.16E+11	0.450
	M8-T10	550	0.021	2.11E+11	1.08E+11	0.488
	M8-T10	550	0.041	2.11E+11	9.70E+10	0.540
	M8-T11	700	0.009	2.00E+11	8.17E+10	0.592
	M8-T11	700	0.021	2.00E+11	7.29E+10	0.636
	M8-T11	700	0.041	2.00E+11	6.42E+10	0.679
	M9-T03	20	0.000	2.02E+11	2.02E+11	0.000
	M9-T03	20	0.009	2.02E+11	1.83E+11	0.094
	M9-T03	20	0.021	2.02E+11	1.65E+11	0.183
	M9-T03	20	0.041	2.02E+11	1.46E+11	0.277
	M9-T08	400	0.009	2.14E+11	1.71E+11	0.201
	M9-T08	400	0.021	2.14E+11	1.60E+11	0.252
M9	M9-T08	400	0.041	2.14E+11	1.46E+11	0.318
	M9-T15	550	0.009	2.10E+11	1.21E+11	0.424
	M9-T15	550	0.021	2.10E+11	1.14E+11	0.457
	M9-T15	550	0.041	2.10E+11	1.02E+11	0.514
	M9-T20	700	0.009	2.14E+11	9.42E+10	0.560
	M9-T20	700	0.021	2.14E+11	7.00E+10	0.673
	M9-T20	700	0.041	2.14E+11	5.66E+10	0.736

TABLE 2. Damage parameters best fit to tensile coupon test results

Test series	Best-fit damage parameters							
	S	p_D	a	b	c	r	m	k
M7	4.98E+05	0.004	4.375	-1213.75	-20	0.695	1.864	0.064
M8	5.66E+05	0.004	2.334	-915.7	-20	0.786	4.99	0.125
M9	4.75E+05	0.004	1.952	-837.323	-20	0.613	3.01	0.248

TABLE 3. Damage parameters employed in steel tubular truss analysis

S	p_D	a	b	c	r	m	k
1.72E+05	0.01	2.81	-1027	-20	0	9.63	4

TABLE 4. Damage parameters recommended for use in structural fire engineering

| Heating rate | Damage parameters | | | | | | | |
	S	p_D	a	b	c	r	m	k
> 10°C/min	1.72E+05	0.01	2.81	-1027	-20	0	9.63	4
≤ 10°C/min	4.75E+05	0.004	1.952	-837.323	-20	0.613	3.01	0.248

List of Figures

33

Fig. 1. Thermal damage variable $h(T)$ determined from literature sources
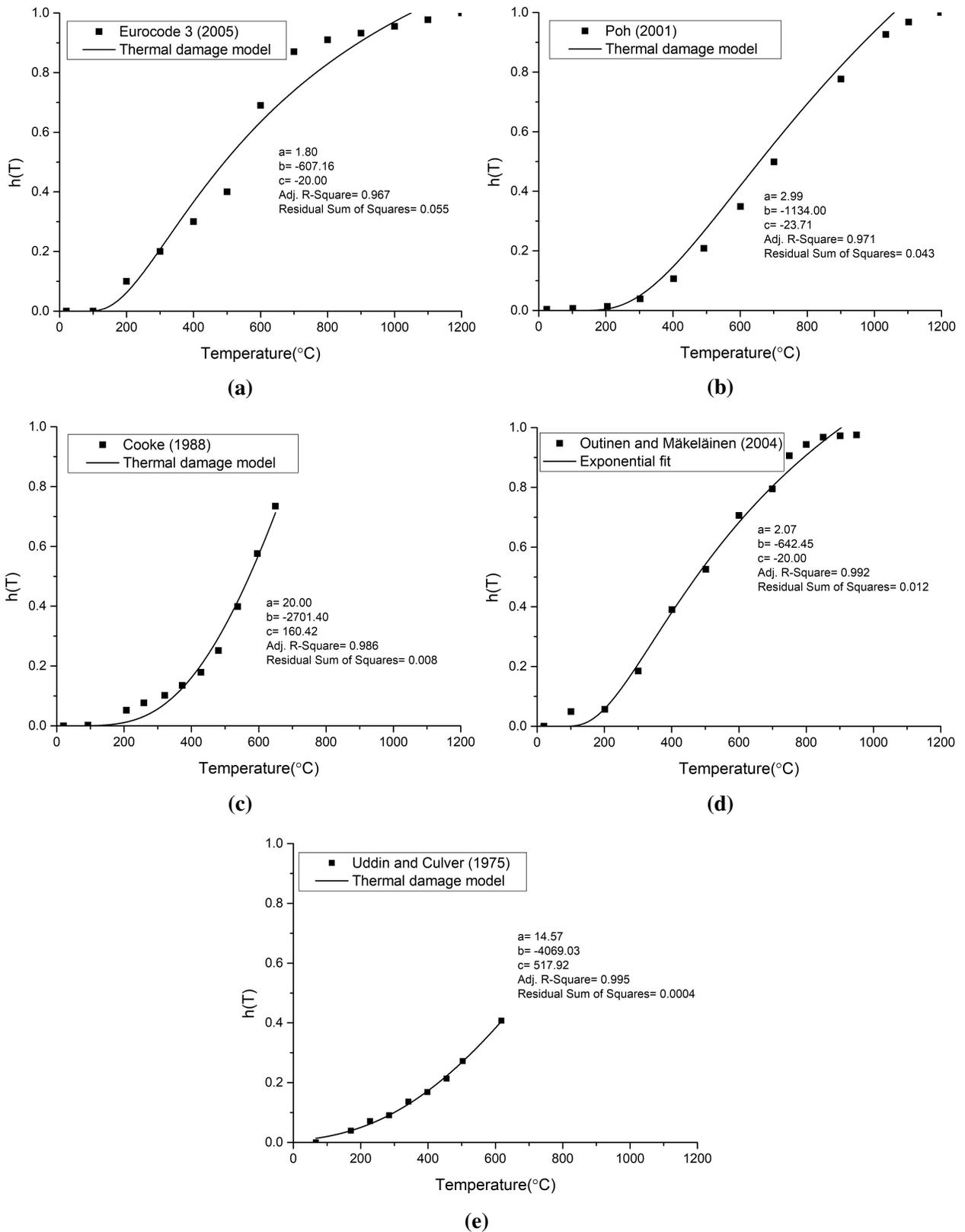
Fig. 2. Plots of the proposed thermal damage model with parameters best fit to experimental results and EC3 model
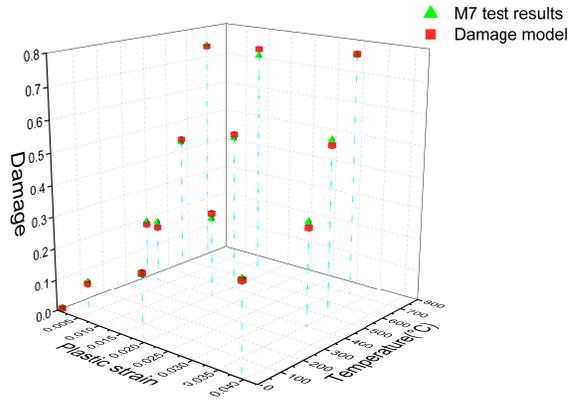
(a) M7
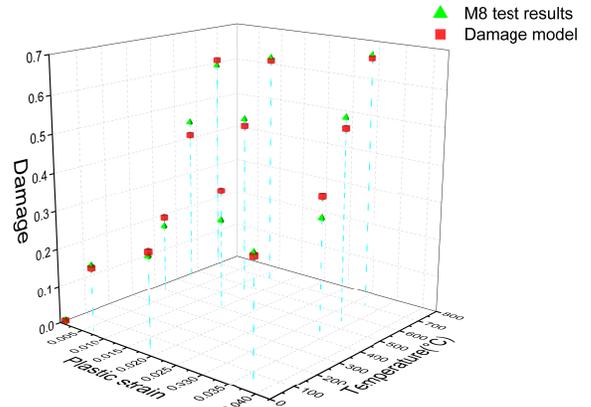
(b) M8
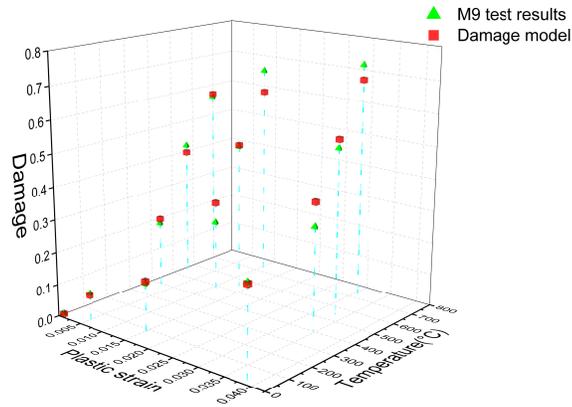
(c) M9

Fig. 3. Comparison between test results and the damage model prediction with best-fit parameters

36
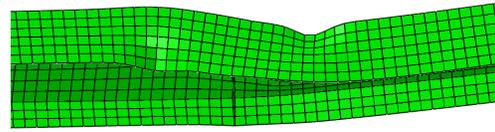
(a) Dharma and Tan (2007)   (b) Damage model prediction

Fig. 4. Local and lateral torsional buckling of specimen S3-1
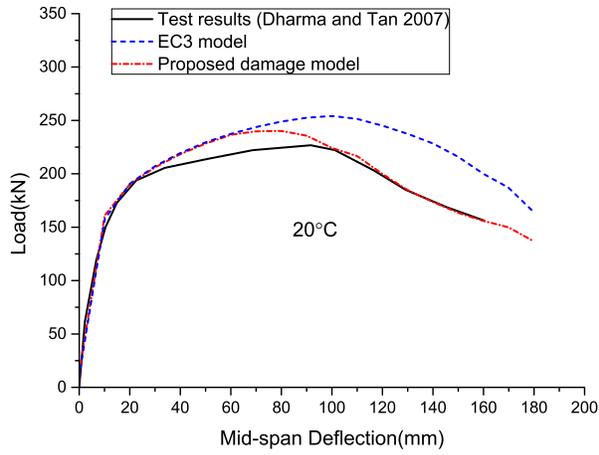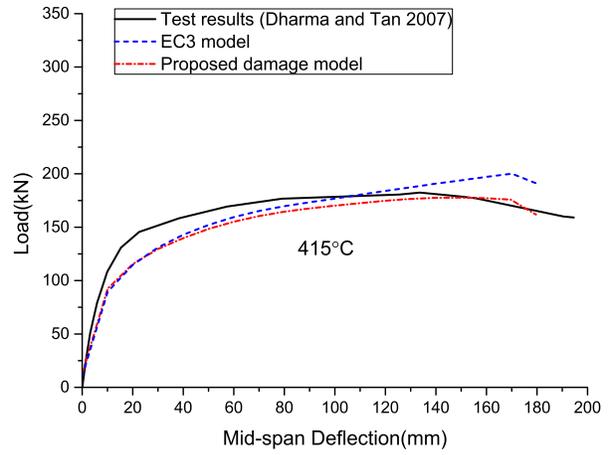
(a) specimen S3-1　　　　　　　　　　　**(b)** specimen S3-2
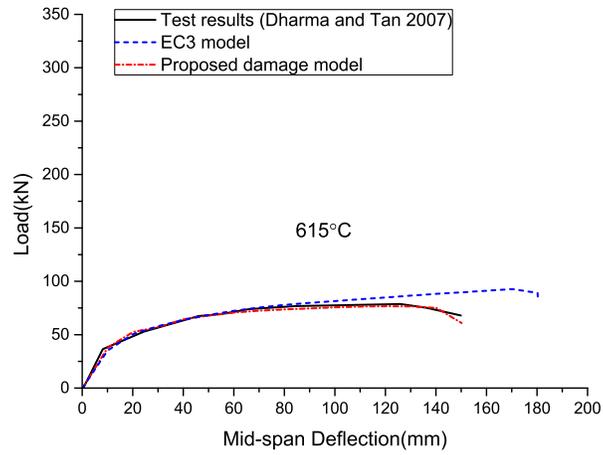
(c) specimen S3-3

Fig. 5. Load-deflection histories of beam specimens at mid-span
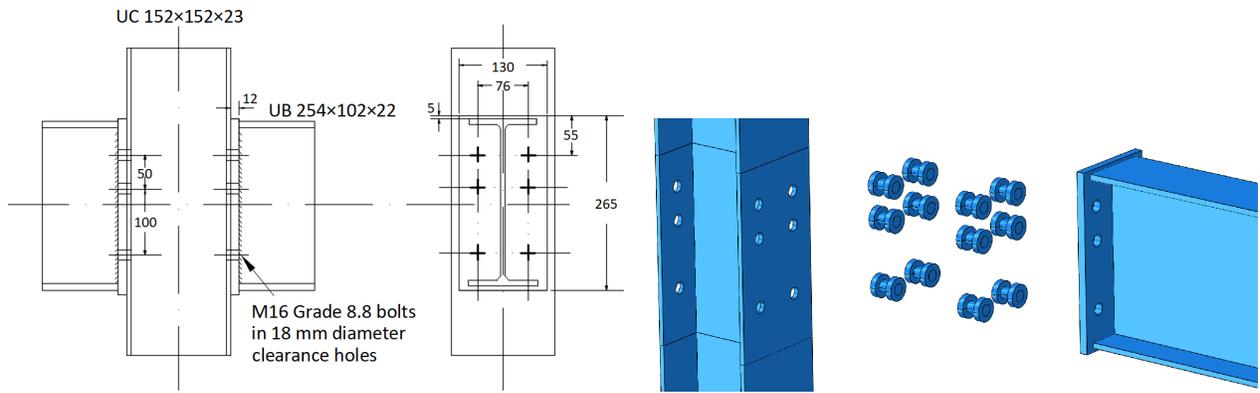
(a) Geometric layout (Leston-Jones et al. 1997)

(b) Assembling of connection components

Fig. 6. Modelling details of flush end plate connection

(a) Ambient test (Leston-Jones et al. 1997)
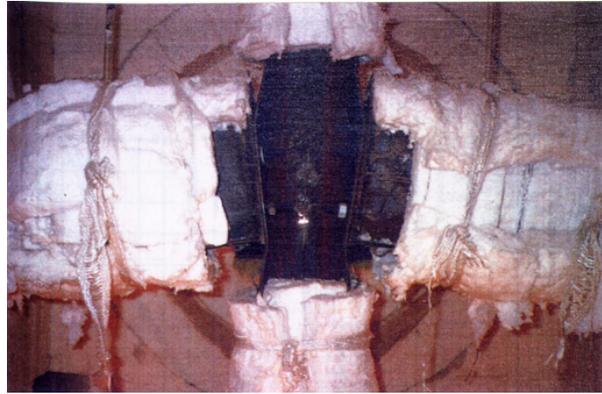
(b) Fire test 1 (Leston-Jones et al. 1997)
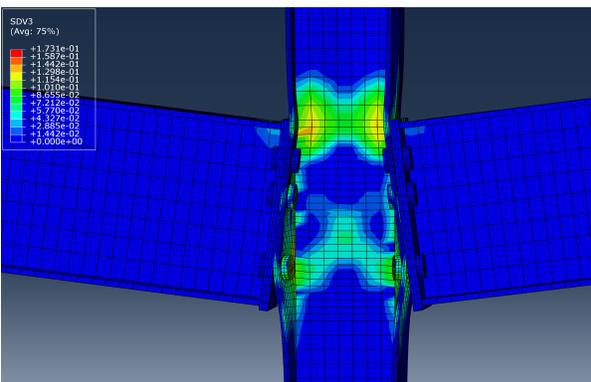
(c) Damage model prediction of ambient test
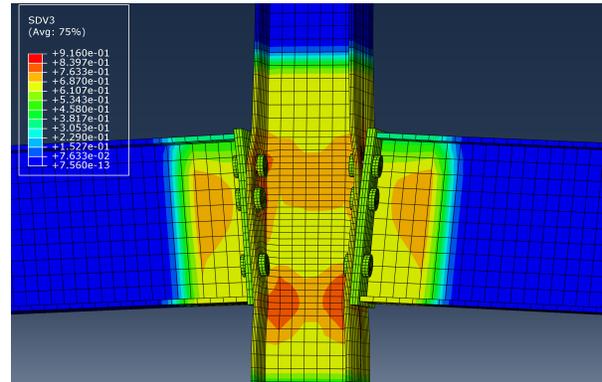
(d) Damage model prediction of fire test 1

Fig. 7. Comparison of connection failure modes
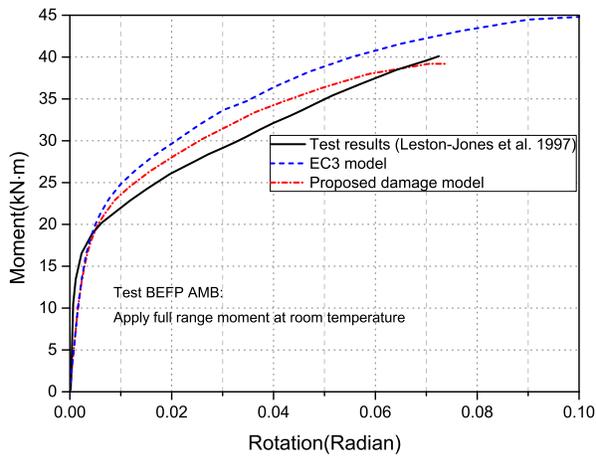
(a) ambient-temperature test (BFEP AMB)
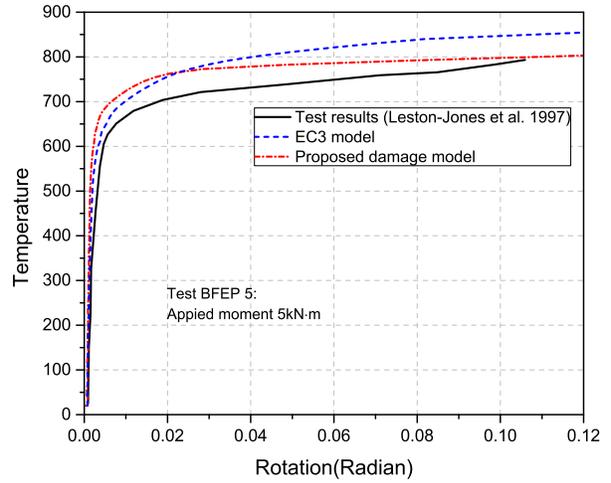
(b) fire test 1 (BFEP5)
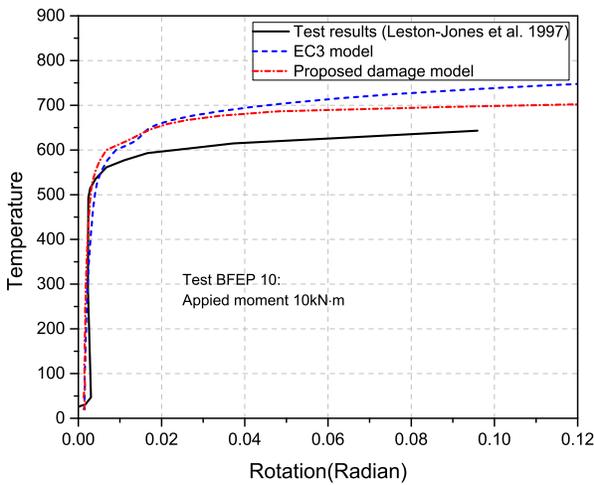
(c) fire test 2 (BFEP10)
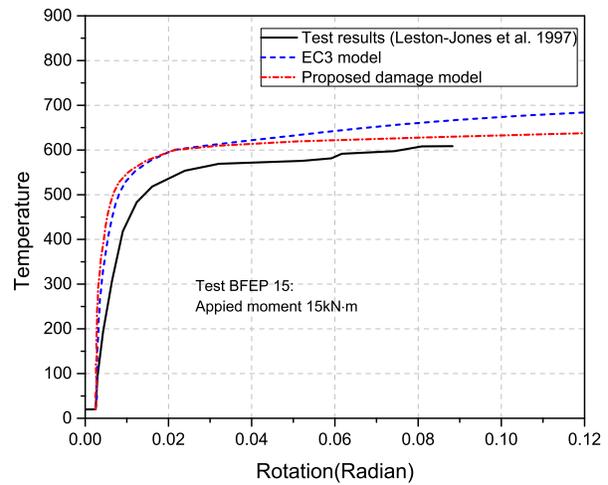
(d) fire test 3 (BFEP15)
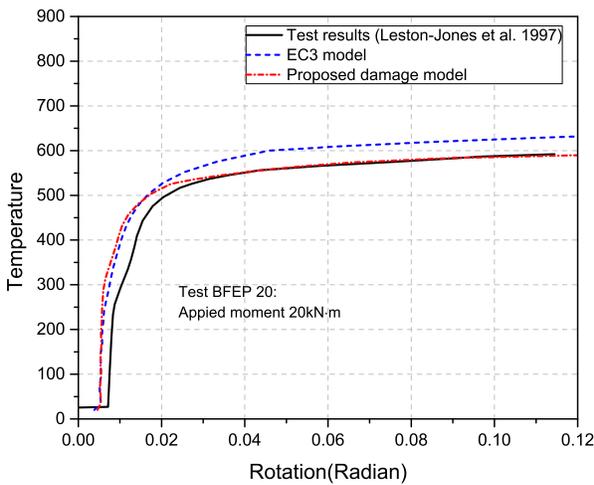
(e) fire test 4 (BFEP20)
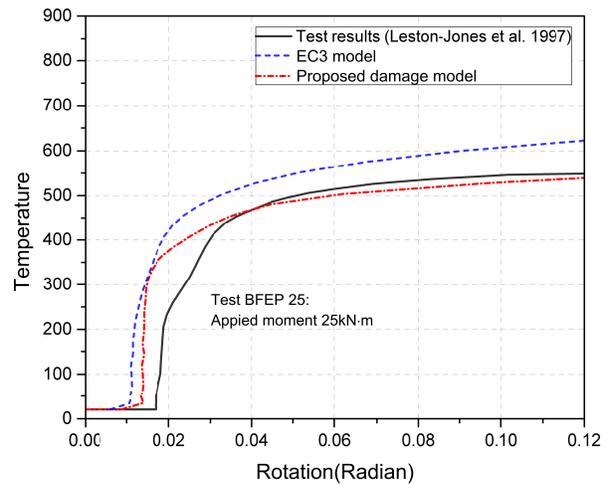
(f) fire test 5 (BFEP25)

**Fig. 8.** Comparison of connection responses between numerical cases and test results

41
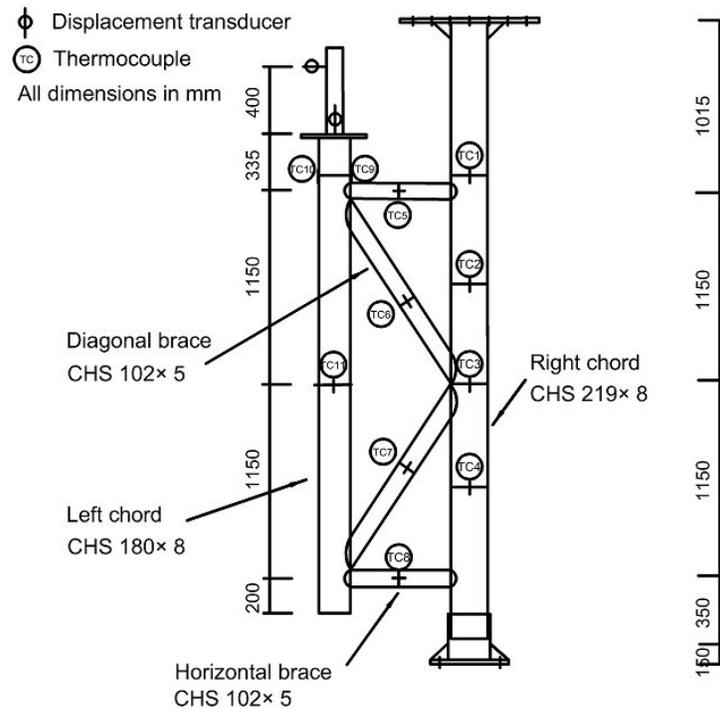
Fig. 9. Steel tubular truss test set-up (Liu et al. 2010)

**(a)** specimen SP1   **(b)** specimen SP2
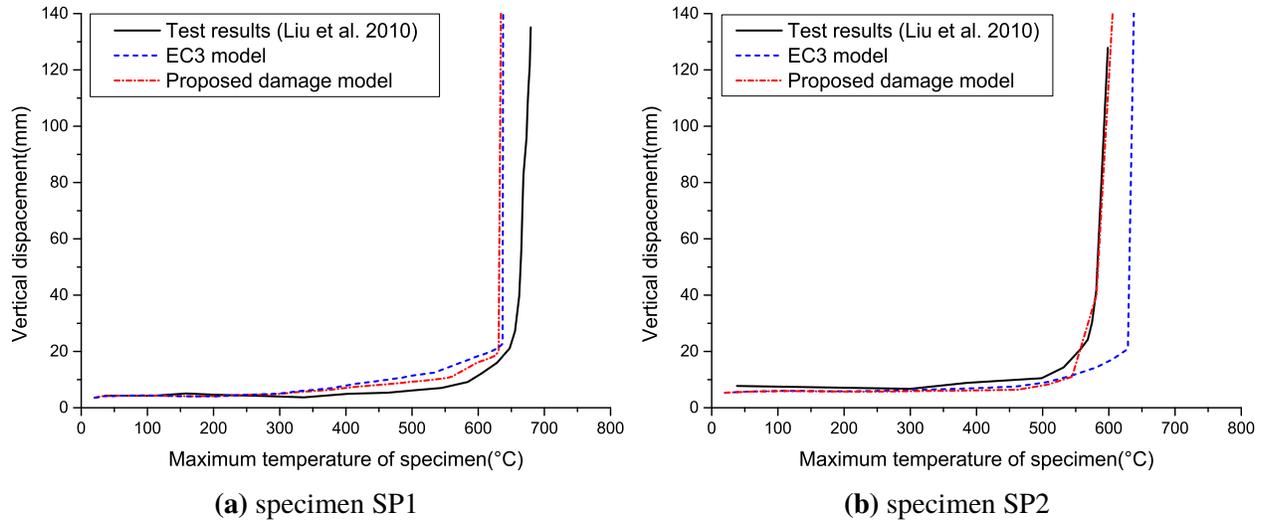
Fig. 10. Vertical displacement versus maximum temperature curve of specimen SP1 and SP2